p16 Represses DNA Damage Repair via a Novel Ubiquitin-Dependent Signaling Cascade

David P. Molkentine[1], Jessica M. Molkentine[1], Kathleen A. Bridges[2], David R. Valdecanas[2], Annika Dhawan[1], Reshub Bahri[1], Andrew J. Hefner[1], Manish Kumar[3], Liangpeng Yang[4], Mohamed Abdelhakiem[1], Phillip M. Pifer[1], Vlad Sandulache[5], Aakash Sheth[6], Beth M. Beadle[7], Howard D. Thames[4], Kathryn A. Mason[2], Curtis R. Pickering[8], Raymond E. Meyn[2,†], and Heath D. Skinner[1]

ABSTRACT

Squamous cell carcinoma driven by human papillomavirus (HPV) is more sensitive to DNA-damaging therapies than its HPV-negative counterpart. Here, we show that p16, the clinically used surrogate for HPV positivity, renders cells more sensitive to radiotherapy via a ubiquitin-dependent signaling pathway, linking high levels of this protein to increased activity of the transcription factor SP1, increased HUWE1 transcription, and degradation of ubiquitin-specific protease 7 (USP7) and TRIP12. Activation of this pathway in HPV-positive disease led to decreased homologous recombination and improved response to radiotherapy, a phenomenon that can be recapitulated in HPV-negative disease using USP7 inhibitors in clinical development. This p16-driven axis induced sensitivity to PARP inhibition and potentially leads to "BRCAness" in head and neck squamous cell carcinoma (HNSCC) cells. Thus, these findings support a functional role for p16 in HPV-positive tumors in driving response to DNA damage, which can be exploited to improve outcomes in both patients with HPV-positive and HPV-negative HNSCC.

Significance: In HPV-positive tumors, a previously undiscovered pathway directly links p16 to DNA damage repair and sensitivity to radiotherapy via a clinically relevant and pharmacologically targetable ubiquitin-mediated degradation pathway.

Introduction

Human papillomavirus (HPV) drives development of cervical, anal, penile and head and neck squamous cell carcinoma (HNSCC; refs. 1–3). Annually, 630,000 cancer cases are related to HPV, with recent and dramatic increases in HPV-related HNSCC (3–6). Clinical outcomes following standard-of-care radiotherapy and platinum-based chemotherapy in HNSCC are far better for HPV-positive(+) versus HPV-negative(−) tumors (7, 8). Also, HPV(+) cell lines are more sensitive to radiotherapy than HPV(−) lines (9–13). These findings suggest an inherent mechanism by which HPV infection confers sensitivity to genotoxic therapy through the DNA damage response (DDR) pathway (14).

A hallmark of HPV infection is overexpression of p16 (7, 15–17), a consequence of E7-dependent pRb inhibition and degradation. Indeed, this protein is a surrogate biomarker for HPV in clinical settings (15). p16 regulates the cell-cycle (18), cell response to DNA damage (19–21), and cellular senescence following genotoxic exposure (22). Although thought nonfunctional in HPV(+) cancers, we found that overexpression of p16 can simulate HPV-dependent radioresponse, suggesting that this phenomenon is dependent on p16 (12, 21). Understanding p16′s ability to modulate the radiosensitivity could lead to strategies to enhance the response of HPV (−) tumors and perform rational treatment de-intensification in HPV(+) tumors.

We established that p16 can modulate the response to DNA damage via control of TRIP12 (12), a HECT domain ubiquitin E3 ligase. TRIP12 binds to and inhibits RNF168—an E3 ligase RING finger protein—and prevents excessive spreading of 53BP1-specific DNA repair foci by controlling extent of chromatin ubiquitination at sites of DNA damage (23). Cells expressing p16 have significantly downregulated levels of TRIP12 (12) and enlarged 53BP1 foci in response to radiotherapy (23). Thus, p16 leads to a decrease in TRIP12 that compromises DNA repair, specifically the repair of DNA double-strand breaks (DSB) by homologous recombination (HR). Considering these findings, we proposed an inverse relationship between p16 and TRIP12 partially explaining the sensitivity of HPV(+) tumors to radiotherapy. It is currently unknown neither how p16 might regulate TRIP12 nor if this pathway is clinically relevant. To address these questions, we comprehensively evaluated the function of p16 in HNSCC and identified a novel p16–HUWE1–USP7–TRIP12 pathway

[1]Department of Radiation Oncology, University of Pittsburgh, UPMC Hillman Cancer Center, Pittsburgh, Pennsylvania. [2]Department of Experimental Radiation Oncology, The University of Texas MD Anderson Cancer Center, Houston, Texas. [3]Department of Biochemistry, AIMS, Bilaspur, Himachal Pradesh, India. [4]Department of Radiation Oncology, The University of Texas MD Anderson Cancer Center, Houston, Texas. [5]Department of Otolaryngology-Head and Neck Surgery, Baylor College of Medicine, Houston Texas. [6]Department of Internal Medicine, Baylor College of Medicine, Houston Texas. [7]Department of Radiation Oncology, Stanford University, Stanford California. [8]Department of Head and Neck Surgery, The University of Texas MD Anderson Cancer Center, Houston, Texas.

Note: Supplementary data for this article are available at Cancer Research Online (http://cancerres.aacrjournals.org/).

[†]Deceased.

D.P. Molkentine and J.M. Molkentine contributed equally as co-authors of this article.

K.A. Mason is retired.

Corresponding Author: Heath D. Skinner, UPMC Hillman Cancer Center, 5117 Centre Avenue, Suite 2.6, Pittsburgh, PA 15213. Phone: 412-623-3275; E-mail: skinnerh@upmc.edu

Cancer Res 2022;82:916–28

doi: 10.1158/0008-5472.CAN-21-2101

repressing HR and associated with survival. Activation of this pathway may be associated with "BRCAness" in HNSCC and provide a biomarker of PARP sensitivity, whereas repression of this pathway could be reversed using USP7 inhibitors currently under development to improve responses to radiotherapy.

Materials and Methods

Cell lines and culture conditions

HNSCCs HN5 (NCBI_Iran Cat# C196, RRID:CVCL_8128), HN30 (RRID:CVCL_5525), HN31 (RRID:CVCL_5526), UM-SCC-1 (Millipore Cat# SCC070, RRID:CVCL_7707), UM-SCC-25 (RRID:CVCL_7735), and UM-SCC-47 (Millipore Cat# SCC071, RRID:CVCL_7759) were obtained from Dr. Jeffrey Myers (UT MD Anderson). HEK-293T (KCB Cat# KCB 200744YJ, RRID:CVCL_0063), FaDu (DSMZ Cat# ACC-784, RRID:CVCL_1218), UPCI:SCC-152 (ATCC Cat# CRL-3240, RRID:CVCL_C058), UPCI:SCC-154 (ATCC Cat# CRL-3241, RRID:CVCL_2230), NCI-H460 (NCI-DTP Cat# NCI-H460, RRID:CVCL_0459), NCI-H1299 (NCI-DTP Cat# NCI-H1299, RRID:CVCL_0060), and Detroit 562 (CLS Cat# 300399/p754_Detroit-562, RRID:CVCL_1171) cells were purchased from the ATCC. At every new frozen batch generation, DNA fingerprinting, and *Mycoplasma* testing were performed by the Cancer Center Support Grant-funded Characterized Cell Line core at MD Anderson (CA016672) or by IDEXX BioAnalytics. HN5, HN30, HN31, and UM-SCC-1 cells were cultured in DMEM/F-12 (Mediatech) supplemented with 10% heat-inactivated (56°C, 30 minutes) FBS (Sigma) and 1% Pen-Strep (Gibco). NCI-H460 and NCI-H1299 cells were cultured in RPMI-1640 (Gibco) supplemented with 10% heat-inactivated FBS and 1% Pen–Strep. UM-SCC-47 cells were cultured in DMEM (Gibco) supplemented with 10% heat-inactivated FBS, 1% Pen–Strep, 2% MEM vitamins (Gibco), 1% sodium pyruvate (Lonza), and 1% non-essential amino acids (Gibco). FaDu, Detroit 562, UPCI:SCC-152 and UPCI:SCC-154 were grown in MEM (Gibco) with 10% heat-inactivated FBS, 1% Pen–Strep and 1% sodium pyruvate. All cells were incubated at 37°C, 5% carbon dioxide.

For cell line authentication and *Mycoplasma* testing after September 2018, each time a new batch of cells is frozen, one vial from that batch is sent to IDEXX BioAnalytics for cell line authentication and pathogen testing (CellCheck 9: 9-Marker STR Profile and Interspecies Contamination Test with *Mycoplasma* testing) before use. In addition, for cell lines used *in vivo*, IMPACT III PCR Profile for Ectromelia, EDIM, LCMV, LDEV, MHV, MNV, MPV, MVM, *Mycoplasma* pulmonis, *Mycoplasma* sp., Polyoma, PVM, REO3, Sendai, TMEV is performed.

For cell line authentication and *Mycoplasma* testing before September 2018, each time a new batch of cells is frozen, one vial from that batch is sent to MD Anderson Cancer Center Characterized Cell Line Core for cell line authentication (STR DNA Fingerprinting using Promega Power PLex 16HS Kit) before use. In addition, for cell lines used *in vivo*, IMPACT III PCR Profile for Ectromelia, EDIM, LCMV, LDEV, MHV, MNV, MPV, MVM, *Mycoplasma* pulmonis, *Mycoplasma* sp., Polyoma, PVM, REO3, Sendai, TMEV is performed by IDEXX BioAnalytics.

Typically, cell lines are kept out in culture and used for about 2–3 months. After this time, the cells would be discarded and a new vial would be thawed for use.

Clonogenic survival assays

Clonogenicity was tested following radiotherapy using an X-RAD 320 biological irradiator (Precision X-Ray) as previously described (12). Briefly, single cells were plated into 6-well dishes and incubated overnight. The next day, the cells were irradiated and then returned to the incubator for 10–21 days until colonies formed. Colonies with more than 50 cells were counted. Survival curves were generated by extrapolation from radiotherapy surviving fractions using alpha/beta analysis with GraphPad Prism v9 (GraphPad Prism, RRID:SCR_002798). Each experiment was plated in triplicate and repeated at least three independent times. Error bars represent standard error.

Clonogenicity was tested following drug (GNE-6640 and/or olaparib; Selleck Chemicals) treatment. For combination GNE-6640 and olaparib, cells were treated with GNE-6640 in T25 flasks for 48 hours. After 48 hours, cells were seeded into 6-well dishes containing GNE-6640 or GNE-6640 plus olaparib for 72 hours. For p16-modulation and olaparib experiments, cells were seeded into 6-well dishes. The next day, cells were treated with increasing doses of olaparib (Selleck Chemicals) for a total of 72 hours. In both sets of experiments, after 72 hours wells were replaced with fresh drug-free media and left for a total of 9–10 days for HN5 or 14–17 days for UM-SCC-47. Colonies were stained with 0.25% crystal violet (Sigma) in methanol and colonies with more than 50 cells were counted. Plots were generated using GraphPad Prism v9.

3-[4,5-dimethylthiazol-2-yl]-2,5 diphenyl tetrazolium bromide (MTT) assay

Cell concentration was normalized to 10,000 cells/mL. A total of 1,000 cells (100 μL) were seeded per well into 96-well plates. The next day, drugs at gradient concentrations were diluted to 10X concentration and 11 μL/well was added to the 100 μL media and cells. After 72 hours drug treatment, 50 μL 5 mg/mL Thiazolyl Blue Tetrazolium Bromide solution (Sigma, MTT) was added for 3 hours. Wells were aspirated and 150 μL DMSO was added for 30 minutes on shaker. Plates were read using an Epoch Microplate Spectrophotometer (BioTek) at 590 nm and Gen5 v.3.05 software (Gen5, RRID:SCR_017317). Plots were generated using GraphPad Prism v9.

Antibodies and reagents

USP7 (Abcam Cat# ab4080, RRID:AB_2214019), RNF168 (Abcam Cat# ab151955, RRID:AB_2893475), ARF-BP1 (HUWE1; Abcam Cat# ab70161, RRID:AB_1209511), and TRIP12 (Abcam Cat# ab86220, RRID:AB_1925533) antibodies were purchased from Abcam; p16 antibody from BD Biosciences (BD Biosciences Cat# 554079, RRID:AB_395229); BRCA1 (Santa Cruz Biotechnology Cat# sc-6954, RRID:AB_626761) and alpha tubulin (Santa Cruz Biotechnology Cat# sc-5286, RRID:AB_628411) from Sant Cruz Biotechnology; and HA (BioLegend Cat# 660001, RRID:AB_2563417) from BioLegend; K48-linked ubiquitin (Millipore Cat# 05–1307, RRID:AB_1587578) from Millipore; K63-linked ubiquitin (Cell Signaling Technology Cat# 5621, RRID:AB_10827985) and Aurora Kinase A (Cell Signaling Technology Cat# 3092, RRID:AB_2061342) from Cell Signaling Technology; and Actin (Millipore Cat# MAB1501, RRID:AB_2223041) from Millipore. MG132 was purchased from Cell Signaling Technology, and cells were treated with doses ranging from 5–10 μmol/L for 5–12 hours. Cycloheximide was purchased from Sigma-Aldrich, and cells were treated with 300 μg/mL for the times indicated. GNE-6640 was purchased from MedChemExpress, and cells were treated with doses ranging from 0.1 to 10 μmol/L for 6 to 48 hours before irradiation and left on until collection or staining of cells. P5091 was purchased from Sigma-Aldrich, and cells were treated with doses ranging from 1 to 5 μmol/L for 1 hour before and 18 hours after irradiation.

Western blot analysis

Following treatment, cells were lysed with extraction buffer containing 20 mmol/L HEPES (pH 7.9), 0.4 mmol/L NaCl, 1 mmol/L EDTA (pH 8.0), and 1 mmol/L EGTA (pH 7.0). XPert protease and phosphatase inhibitors were added at a 1:100 dilution (GenDepot) and then sonicated. Equal amounts of protein were loaded into 4%–15% gradient polyacrylamide gels (Bio-Rad) and then transferred to polyvinylidene difluoride (PVDF) membranes for 10 minutes at 25 V using a Trans-Blot Turbo (Bio-Rad). Membranes were incubated in 5% dry milk in TBS + 0.1% TWEEN 20 (Sigma) for 1 hour and then incubated with primary antibody overnight at 4°C. Immunoblots were detected using horseradish peroxidase–conjugated secondary antibodies (GE) and ECL2 chemiluminescent substrate (Pierce). Densitometry was measured using ImageJ (RRID:SCR_003070). Western blots for TRIP12 were always run on the same day the cells were collected due to the instability of TRIP12 protein.

Overexpression and shRNA lentiviral infection

pLenti puro HA-Ubiquitin was a gift from Melina Fan (RRID: Addgene_74218). Stable overexpression of USP7 (OHS5897–202624117), p16 (Horizon OHS5898; ref. 12) or rfp pLOC Turbo lentiviral vector (OHS5832; Precision LentiORF, Horizon) or stable shRNA knockdown of USP7 (RHS4430–200175624, RHS4430–200287423, RHS4430–200297458), p16 (RHS4430–200288758, RHS4430–200290001), HUWE1 (RHS4430–200172491) or TRIP12 (RHS4430–200172790, RHS4430–200198676, RHS4430–200196018) GIPZ lentiviral shRNA or GIPZ nonsilencing lentiviral shRNA control (RHS4346; Horizon) were cotransfected with lentiviral particles DR.8 (RRID:Addgene_8455) and VSVG (RRID:Addgene_8454; Addgene) in HEK-293T cells for 48 hours using Fugene (Promega) transfection reagent. Media plus lentivirus were then filtered through a 0.45-μm PES syringe filter and added to cells. Polybrene (5 μg/mL) was added, and the cells were transduced for 6 hours. The transduction procedure was repeated for 2 consecutive days. Three days after initial transduction, stably expressing cells were selected with either 20 μg/mL blasticidin (overexpression) or 2 μg/mL puromycin (shRNA).

siRNA transfection

siRNA was transfected using Nucleofector II technology (Amaxa). Briefly, 1 million cells were resuspended in 100 μL Reagent T (Lonza) and 200 nmol/L siRNA (Dharmacon). Cells were electroporated with program T-001, plated in 6-well dishes containing complete media, and collected at the times indicated.

P16 CRISPR

A single colony of the LentiCRISPRv2 plasmid (RRID:Addgene_52961) was expanded in LB broth containing 100 μg/mL ampicillin, and plasmid DNA was isolated using the QIAfilter Plasmid Midi Kit (Qiagen). The plasmid was then linearized and dephosphorylated by BsmBl digestion, ran on 0.8% agarose gel, and purified with a QIAquick Gel Extraction Kit (Qiagen). p16 guide RNA, sgCDKN2A CACCGTTCGGCTGACTGGCTGGCCA, and reverse complement, AAACTGGCCAGCCAGTCAGCCGAAC (Sigma), were annealed by PCR. gRNA was ligated into the purified LentiCRISPRv2 plasmid (RRID:Addgene_52961) and transformed into One shot Stbl3 Chemically Competent *E. coli* (#C7373–03, Thermo Fisher Scientific). A single clone was then selected, propagated, and Sanger sequenced to confirm the insert. The sg-p16 CRISPR plasmid was then cotransfected with DR.8 and VSVG in HEK-293T cells for 48 hours using Fugene (Promega) transfection reagent. Media containing lentivirus were then filtered through a 0.45-μm PES syringe filter and added to cells. Polybrene (5 μg/mL) was added, and the cells were transduced for 6 hours. The transduction procedure was repeated for 2 consecutive days. Three days after initial transduction, stably expressing cells were selected with 2 μg/mL puromycin.

RT-PCR

Cells were collected and then lysed using a QIAshredder Kit (Qiagen). RNA extraction was performed using an RNeasy Kit (Qiagen), and RNA was quantified on a Take3 plate (BioTek) and read on an Epoch spectrophotometer (BioTek). Reverse transcription was performed using iScript Reverse Transcription Supermix (Bio-Rad) with 1 μg of total RNA/reaction. 50 ng of cDNA template was mixed with primers and SsoAdvanced Universal SYBR Green Supermix (Bio-Rad). PrimePCR primer sets for GAPDH, HUWE1, TRIP12 or USP7 were purchased from Bio-Rad. Real-time PCR was run on a CFX Connect Real-Time PCR system (Bio-Rad). Data were normalized to GAPDH.

Immunocytochemistry

Cells were plated directly on a coverslip and allowed to adhere with overnight incubation. The following day, the cells were irradiated and fixed with 4% paraformaldehyde for 10 minutes at room temperature. Cells were then washed with PBS and permeabilized with 70% ethanol overnight at 4°C and for 20 minutes with 0.1% Igepal at room temperature. Cells were washed, blocked with 2% BSA for 1 hour and incubated overnight with 1:1,000 Aurora Kinase A antibody (Cell Signaling Technology). Centrosomes were visualized by 1 hour incubation with a 1:500 AlexaFluor 594 fluorochrome (Invitrogen). Cells were then incubated with 1:500 alpha tubulin (Santa Cruz Biotechnology) for 1 hour at room temperature. Mitotic spindles were visualized by 1 hour incubation with 1:600 FITC (Jackson ImmunoResearch), and DNA was stained with 1 μg/mL DAPI (RRID: AB_2893474; Sigma). Pictures were captured with a Leica microscope.

BRCA1 foci were visualized by incubating 1:500 BRCA1 antibody overnight (Santa Cruz Biotechnology) and 1:600 FITC (Jackson ImmunoResearch) for 45 minutes at room temperature. Foci for at least one hundred cells were manually counted per experiment using ImageJ software. Each foci experiment was repeated at least once.

Micronuclei quantification

HN5 cells stably expressing control or shUSP7 constructs were irradiated with 6 Gy and then incubated in medium containing 664 nmol/L nocodazole (Sigma-Aldrich) for 4 hours. At the end of nocodazole treatment, mitotic cells were harvested by gentle shaking and replated on coverslips in media without nocodazole for 24 hours. Cells were then fixed and stained as described above. Plots were generated using GraphPad Prism v9.

Immunoprecipitation

Following treatment, cells were lysed with extraction buffer containing 20 mmol/L Tris-HCl (pH 7.8), 150 mmol/L NaCl, 1 mmol/L EDTA (pH 8.0), and 1 mmol/L EGTA (pH 7.0). XPert protease and phosphatase inhibitors were added at a 1:100 dilution (GenDepot) and then sonicated. One mg of cell lysate per sample was incubated with 5 μg of antibody of interest with rotation at 4°C overnight. Then, 30 μL of 100 mg/mL Protein-A Sepharose beads (GE Healthcare) were added to each sample and rotated at 4°C for 2 hours. The beads were sedimented by centrifugation at 400 rcf, and the bead-bound samples were washed three times with 1 mL lysis buffer. The sample was eluted by heating the bead-bound sample with 25 μL 2X SDS Laemmli Sample Buffer (Bio-Rad) at 100°C for 7 minutes. After centrifugation, each sample was loaded into a 4%–15% gradient polyacrylamide precast gel

(Bio-Rad) and transferred to a PVDF membrane. The resulting sample was analyzed by immunoblot. Immunoprecipitations for TRIP12 were always run on the same day the cells were collected due to the instability of TRIP12 protein.

HR assay

One million HN5 or 3 million UM-SCC-47 cells were electroporated with 5-μg DRGFP (RRID:Addgene_26475) using program T-020 (HN5) or U-026 (UM-SCC-47) in 100 μL reagent kit T (Lonza). After two days of recovery, cells were stably selected with 2 μg/mL puromycin for two weeks, changing drug every other day. For p16 overexpression HR assays, HN5-DRGFP were additionally infected with pLX401-INK4A Tet-ON system (RRID:Addgene_121919) after lentiviral packaging in HEK-293T cells for 48 hours. Cells were grown in media containing Tet system approved FBS (Takara 631107) and infected on two consecutive days.

Three million UM-SCC-47 or 1 million HN5 cells expressing DRGFP were aliquoted into 15-cm centrifuge tubes, pelleted by 300 × *g* centrifugation, and washed one time with 5 mL PBS. Electroporated 2 μg pCAGGS-mCherry (RRID:Addgene_41583) and 6 μg pCBAsceI (RRID:Addgene_26477) plasmids into each group using program T-020 (HN5) or U-026 (UM-SCC-47) in 100 μL reagent kit T (Lonza). For UM-SCC-47 p16 CRISPR group, 2 μg of sg-p16 LentiCRISPRv2 was also cotransfected. HN5-DRGFP-INK4A cells were pretreated with 100 ng/mL doxycycline (Sigma) 48 hours before electroporation. For DRGFP groups, only mCherry was added. After electroporation, cells were transferred to a 6-well dish with 1 mL media containing 10 μmol/L GNE-6640, 100 ng/mL doxycycline, 10 μmol/L ATMi or 100 nmol/L ATRi (Selleck Chem) as indicated. Next day media were changed to 2mL and drug was re-added. 72 hours after electroporation, all cells were trypsinized and collected into 5mL vials, washed 1 time with 1mL PBS, and resuspended in 200–500 μL FACS buffer. Data were collected with BD Accuri C6 flow cytometer. Plots were generated using GraphPad Prism v9.

IP mass spectrometry

Following treatment, cells were lysed with extraction buffer containing 20 mmol/L Tris-HCl (pH 7.8), 150 mmol/L NaCl, 1 mmol/L EDTA (pH 8.0), and 1 mmol/L EGTA (pH 7.0). XPert protease and phosphatase inhibitors were added at a 1:100 dilution (GenDepot) and then sonicated. 25 mg of cell lysate per sample were incubated with 25 μg of antibody of interest with rotation at 4°C overnight. Then, 100 μL of 100 mg/mL Protein-A Sepharose beads (GE Healthcare) were added to each sample and rotated at 4°C for 2 hours. The samples were sedimented by centrifugation, and the bead-bound samples were washed three times in lysis buffer. Beads were then sent to the MD Anderson Proteomics core for mass spectrometry analysis.

Xenograft tumors

HN5 cells were transfected with USP7 shRNA using lentiviral vectors as described above. Two million cells suspended in 20-μL PBS were injected intramuscularly into the right hind leg of 6–8 weeks old, male Swiss Nu/Nu mice (MD Anderson Animal Colony). When tumors reached 8 mm in diameter (range, 7.7–8.3 mm), the animals were randomized into groups and treated with 4 Gy for 5 consecutive days using a Cesium-137 irradiator (dose rate 4 Gy/min). Mice were immobilized in a jig, and tumors were centered in a 3-cm diameter circular field for irradiation. The tumors were then measured every other day until most tumors in a treatment group reached 14 mm in diameter. Animals were euthanized via CO_2 inhalation followed by cervical dislocation. Following euthanasia, the tumors were excised, and a portion of each was snap frozen and formalin fixed.

The time for tumors to reach 11 mm in diameter was used to determine the tumor growth delay (TGD) and dose enhancement factor (DEF). The growth curves for the four conditions shown are approximately linear (coefficient of t^2 not significant for any of the curves), so a linear regression model was used to determine the number of days required for each tumor to reach 11 mm. These data are presented as averages per each treatment group, with significance determined via one-way ANOVA analysis and *post hoc* comparison.

Separately, the enhancement ratio for radiosensitization by USP7 was estimated as the ratio of growth delays between shUSP7 and controls. The calculations were carried out for three diameters (11, 12, and 13 mm) and either for all times or times >6 days to assess the effect of small nonlinearities at the start. Because the observations were not independent (the same tumors are measured at different times), we applied so-called mixture models with random and fixed effects. Linear models where intercept and slope were considered random effects were used in a bootstrapping procedure where data were sampled randomly 100 times and estimates with 95% CIs were obtained from the 2.5- and 97.5-centile distributions. DEF at 11 mm shown in **Fig. 3**, all calculated DEFs had a lower limit of the 95% CI greater than 1 by at least 0.5 arbitrary units.

Clinical data analysis

For expression analysis, HUWE1 mRNA expression was examined for all available patients from The Cancer Genome Atlas (TCGA) Head and Neck cohort for which HPV status was available ($n = 519$). For outcome analysis, data for which HUWE1 mutation status and/or mRNA expression, HPV status and disease-free status were available ($n = 392$). Clinical characteristics (see Supplementary Table S1), outcomes and biologic data were accessed via cBioPortal. Tertiles for HUWE1 expression were determined for the entire study population, then applied to the HPV(+) and HPV(−) cohorts.

Statistical analysis

For quantitative assays a minimum of 3 biological replicates were performed. All *in vitro* experiments were repeated at least once. For *in vitro* and *in vivo* studies either Student *t* test or ANOVA with *post hoc* analysis adjusted for multiple comparisons was used (Prism v8). For clinical data, disease-free survival (DFS) was analyzed using Cox regression analysis. Kaplan–Meier survival curves are shown with log rank statistics used to compare groups for statistical significance.

Study approval

Mouse experiments were carried out in the specific pathogen-free mouse colony of the Department of Experimental Radiation Oncology at MD Anderson Cancer Center and were approved by the American Association for Accreditation of Laboratory Animal Care, in accordance with current regulations and standards of the U.S. Department of Agriculture and the Department of Health and Human Services. Clinical studies were performed using data from TCGA that are publicly available and conforms with recognized ethical guidelines. Informed consent was obtained for all participants in TCGA.

Results

HNSCCs radiosensitivity correlates with TRIP12 and USP7 expression and is HPV-status dependent

We first established that HPV(+) cell lines were significantly more sensitive to radiotherapy than HPV(−) lines examined (**Fig. 1A**) and the HPV(−) cell lines expressed low levels of p16, the surrogate marker

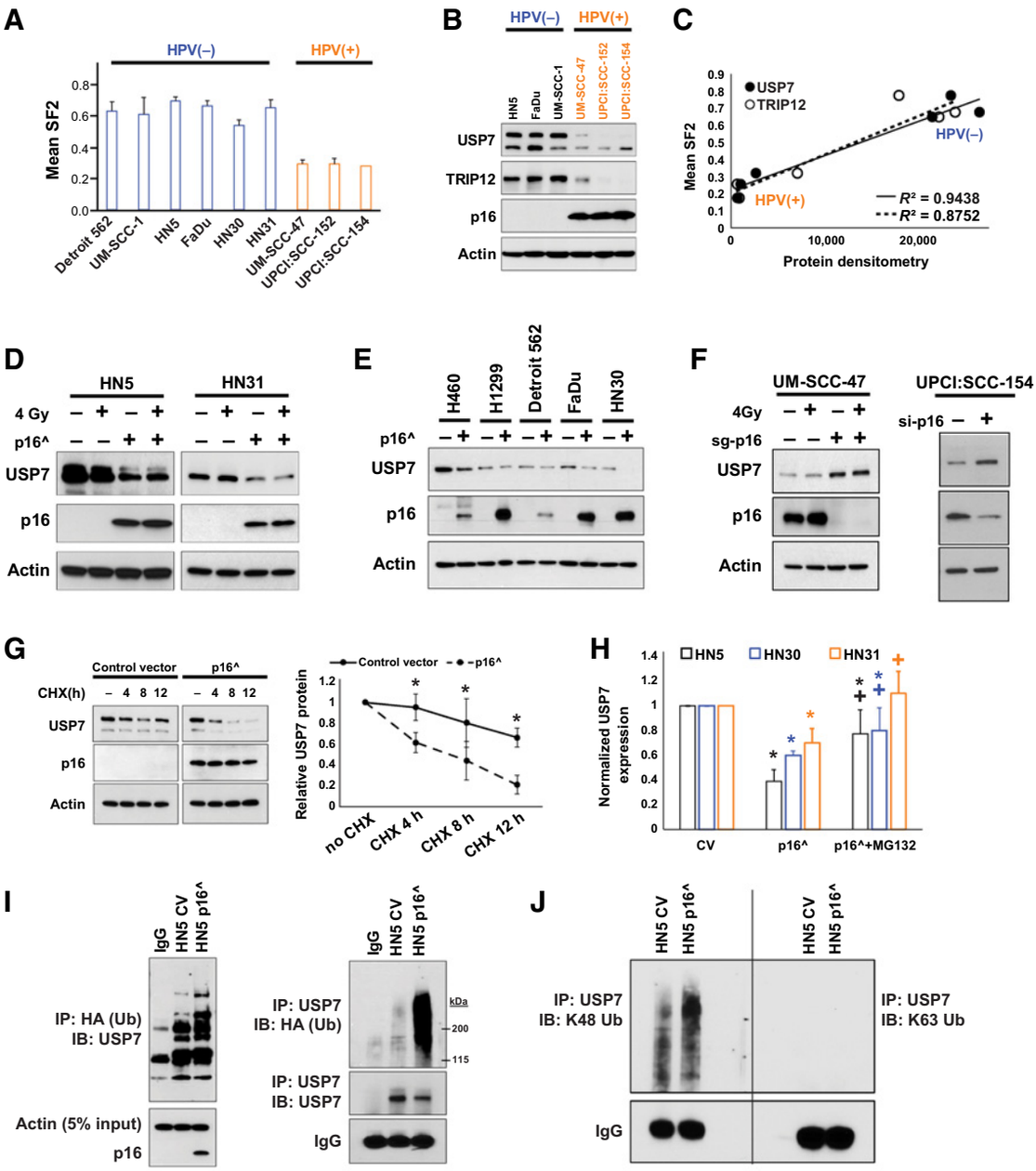

Figure 1.

HNSCC radioresponse and regulation of USP7 by p16. **A** and **B,** Surviving fraction at 2 Gy (SF2; **A**) and immunoblot (**B**) of HPV(−) and HPV(+) cells. **C,** Correlation between SF2 and USP7 (solid dots) or TRIP12 (open dots) protein expression. **D,** Immunoblot following radiotherapy and forced expression of control vector or p16 in HN5 and HN31 HPV(−) HNSCC cell lines. **E,** Immunoblot following forced expression of control vector or p16 in in multiple HPV(−) HNSCC and NSCLC cell types. **F,** Immunoblot following CRISPR KO of p16 in an HPV(+) cell line (UM-SCC-47) and p16 siRNA in a separate HPV(+) cell line (UPCI: SCC-154). **G,** Cyclohexamide (CHX) chase assay in HN5 cells expressing control vector or p16. **H,** MG132 rescue in HPV(−) cells following forced expression of p16 or control vector. Data are densitometry from immunoblots in Supplementary Fig. S1C and are presented as mean ± SEM. Comparisons performed using ANOVA with *post hoc* analysis adjusted for multiple comparisons. *, $P < 0.05$ versus control; +, $P < 0.05$ versus p16 forced expression. **I,** HN5 cells expressing HA-tagged ubiquitin (Ub) and either control vector or p16 were analyzed via IP of HA and immunoblot of USP7 (left) or IP of USP7 and immunoblot of HA (right). **J,** HN5 cells expressing either control vector or p16 were analyzed via IP of USP7, followed by immunoblot for either K48- (left) or K63- (right) linked ubiquitin.

of HPV infection (**Fig. 1B**). In addition, p16 was inversely correlated with TRIP12 (**Fig. 1B**).

We next examined the expression of deubiquitinase ubiquitin-specific protease 7 (USP7), previously shown to bind to TRIP12 (24) and found that USP7 expression was proportional to that of TRIP12 (**Fig. 1B**). In addition, densitometric analysis showed that both USP7 and TRIP12 were highly correlated with radioresistance (**Fig. 1C**).

P16 inhibits USP7 levels by increasing its ubiquitination and degradation

We next examined the impact of p16 modulation on USP7. Although radiotherapy treatment had minimal effects on USP7 protein level, USP7 decreased following forced expression of p16 in HPV(−) cells (**Fig. 1D**) as well as in a larger panel, including both HPV (−) HNSCC and non–small cell lung carcinoma (NSCLC) cell lines (**Fig. 1E**). This panel included TP53 wild-type H460 and HN30 cells. Although not a definitive exploration of p53 in this setting, this observation is suggestive of a possibly p53-independent mechanism across multiple cell types. Conversely, when p16 expression was knocked out via CRISPR in HPV(+) UM-SCC-47 cells, USP7 levels increased (**Fig. 1F**). Similar results were observed following p16 siRNA in a separate HPV(+) cell line (UPCI:SCC-154; **Fig. 1F**). Taken together these findings suggest that p16 regulates USP7 expression.

Next, we sought to determine the mechanism by which p16 regulates USP7. We found that forced p16 expression in HPV(−) HN5, HN30 and HN31 cells had no effect on USP7 mRNA (Supplementary Fig. S1A) despite the reduction seen in protein levels (**Fig. 1D** and **E**); this led us to suspect that the USP7 is regulated via post-translational modification. Therefore, we performed cycloheximide chase assays to determine the effect of p16 expression on the stability of USP7. Although only a limited sampling of the p53 spectra, the presence of p16 significantly destabilized USP7 protein in TP53 mutant HN5 (**Fig. 1G**) and TP53 wild-type HN30 (Supplementary Fig. S1B). We next assessed whether the addition of the proteasome inhibitor MG132 could rescue USP7 following forced expression of p16. MG132 partially rescued p16-induced reduction in USP7 protein in all three lines tested (**Fig. 1H**; Supplementary Fig. S1C), which indicates that the destabilization of USP7 by p16 depends on ubiquitination of USP7. To confirm the role of ubiquitination in this process, HN5 cells were cotransfected with control or p16 and lenti-HA-ubiquitin vectors, then either immunoprecipitated (IP) with HA-tagged ubiquitin and immunoblotted for USP7 or the reverse (**Fig. 1I**). Both assays showed increased ubiquitination of USP7 in the presence of p16 expression, that was K48-linked and not K63-linked (**Fig. 1J**). As K48-linked ubiquitination is associated with degradation (25), this finding suggests that the p16-dependent ubiquitination marks USP7 for degradation.

USP7 stabilizes TRIP12 through deubiquitination

We next IP TRIP12 and immunoblotted for USP7 in HPV(−) HN5 cells as well as the reverse, confirming that USP7 indeed binds to TRIP12 (**Fig. 2A**). In addition, direct targeting of USP7 via shRNA resulted in depression of TRIP12 protein levels in HPV(−) cells (**Fig. 2B**), whereas inhibition of TRIP12 had no effect on USP7 expression (Supplementary Fig. S2A). This indicates that USP7 likely stabilizes TRIP12 and not the converse. The regulation of TRIP12 by USP7 was confirmed in HPV(+) cells, where forced expression of USP7 led to significant upregulation of TRIP12 (**Fig. 2C**), despite the presence of p16, suggesting that p16 regulates TRIP12 through USP7.

Although inhibition of USP7 reduced TRIP12 protein expression, it did not reduce TRIP12 mRNA (Supplementary Fig. S2B), providing evidence that TRIP12 regulation occurs post-translationally. Cycloheximide chase assays in TP53 mutant HN5 and TP53 wild-type HN30 cells both showed a reduced half-life of TRIP12 after USP7 knockdown (**Fig. 2D** and **E**), which, although not a comprehensive evaluation of p53 in this setting, supports a potentially p53-independent mechanism of TRIP12 stabilization by USP7. Treatment with MG132 partially reversed the reduction in TRIP12 protein expression induced by USP7 knockout (**Fig. 2F**; Supplementary Fig. S2C), suggesting that USP7 stabilizes TRIP12 by deubiquitination. In addition, we performed IP for TRIP12 and evaluated HA-tagged ubiquitin, showing that forced expression of p16 increased ubiquitination of TRIP12, which was abolished upon coexpression with USP7 (**Fig. 2G**).

P16 inhibits USP7, leading to repression of HR and enhanced therapeutic sensitivity

To evaluate the therapeutic potential of targeting the putative p16–USP7–TRIP12 axis, we examined the effects of USP7 modulation. Initially, we inhibited USP7 and examined BRCA1 and cell death following radiotherapy treatment. Knockdown of USP7 with shRNA sensitized HN5 cells to radiotherapy (**Fig. 3A**) and reduced BRCA1 expression (**Fig. 3B**). Immunocytochemical analysis of HN5 cells showed that targeting USP7 decreased the formation of BRCA1 foci following radiotherapy exposure, suggesting that in the absence of USP7, repair of radiotherapy-induced DNA damage was compromised (**Fig. 3C**). This reduction in BRCA1 foci seen after inhibition of USP7 caused the cells to progress into mitosis with unrepaired DNA damage, leading to increased mitotic death (Supplementary Fig. S3A–S3C).

In addition, we performed a TGD assay using HPV(−) HN5 xenografts in nude mice as described previously in Materials and Methods. Tumors were excised and analyzed by Western blot, which confirmed shRNA knockdown of USP7 and showed reduced BRCA1 expression (**Fig. 3D**). This *in vivo* model is highly radioresistant, with a total dose of 20 Gy leading to a nonsignificant TGD of 5.22 days ($\pm$6.2) versus untreated control (**Fig. 3E** and **F**). In addition, the inhibition of shUSP7 led to a nonsignificant TGD (4.95 days $\pm$6.2; **Fig. 3E** and **F**). However, the combination of USP7 inhibition and radiotherapy led to a significant TGD compared with all groups (13.7–18.9 days depending upon comparison; **Fig. 3E** and **F**).

To evaluate the therapeutic potential of USP7 inhibition. We next modulated USP7 activity using USP7 inhibitors: GNE-6640, P22077 and P5091. GNE-6640 inhibits the deubiquitinase activity of USP7 with selectivity over a highly structurally similar deubiquitinase (USP47) and a highly active deubiquitinase (USP5; ref. 26). P22077 and P5091 are less selective USP7 inhibitors, also inhibiting USP10 and USP47 (27, 28). Modulating USP7 activity via the chemical inhibitor GNE-6640 resulted in decreased TRIP12 expression (Supplementary Fig. S4A and S4B) and increased radiosensitivity in HPV(−) HN5 cells (**Fig. 3G**). In addition, BRCA1 expression (**Fig. 3H**) and foci formation (**Fig. 3I**) were repressed with the addition of GNE-6640. Similar radiosensitization was achieved using P5091 in HN5 and FaDu cells (Supplementary Fig. S4C and S4D) and P22077 in UM-SCC-25 and FaDu cells at various doses and schedules (not shown).

We next examined the effect of USP7 inhibition on HR in HN5 cells and found that inhibition of USP7 led to a significant reduction in HR (**Fig. 3J**). Because of this reduction, as well as the observed modulation of BRCA1 by USP7, we then examined whether USP7 inhibition could increase sensitivity to PARP inhibition. The combination of olaparib and USP7 inhibition (GNE-6640) led to reduced cell viability (**Fig. 3K**) and clonogenic survival (**Fig. 3L**) in HPV(−) HN5 cells. Specifically, at doses with no inhibitory effect of either agent on MTT assay, the

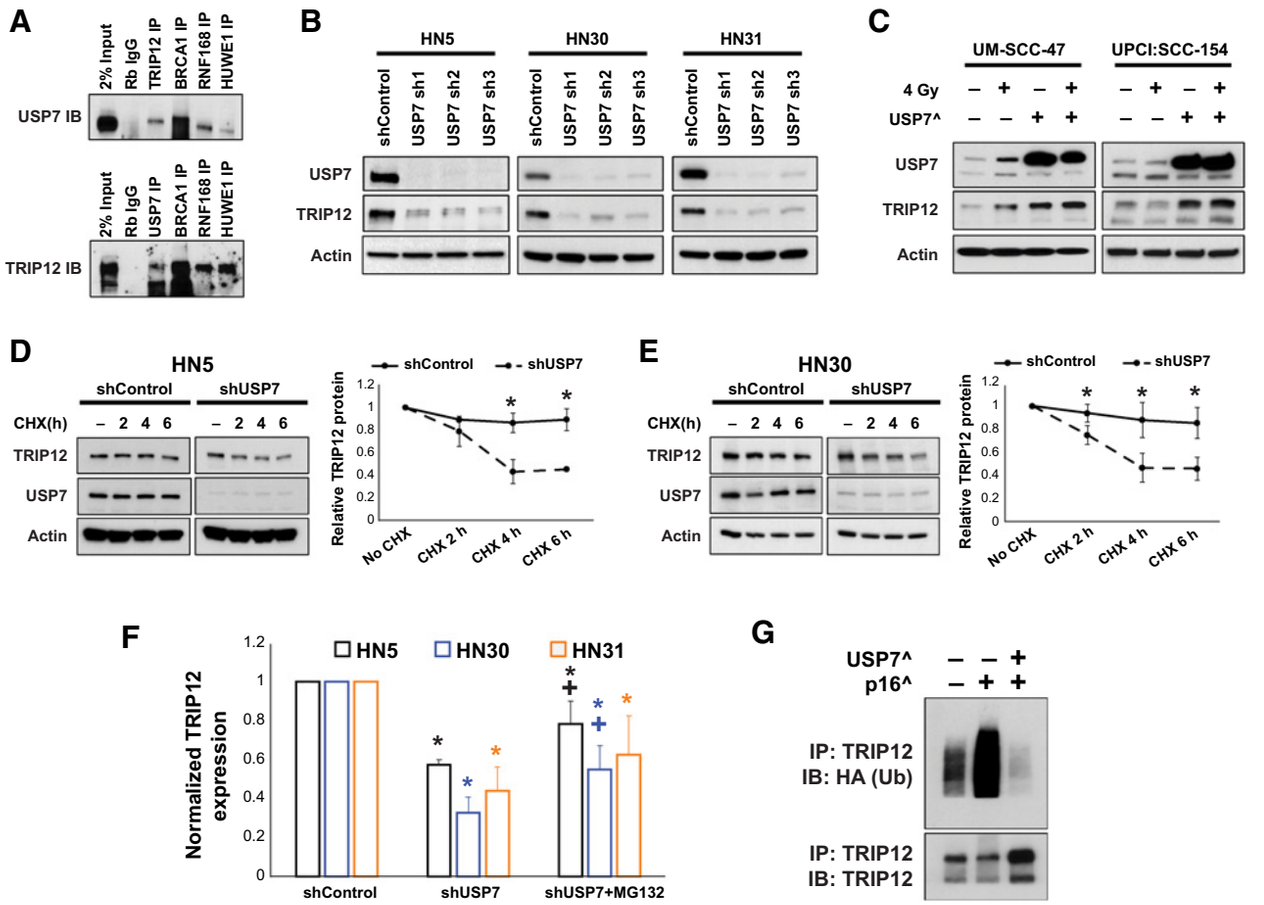

Figure 2.

USP7 stabilizes TRIP12 via deubiquitination. **A,** IP for the indicated proteins in HPV(−) HN5 cells, followed by immunoblot for either USP7 (top) or TRIP12 (bottom). **B** and **C,** Immunoblot of USP7 and TRIP12 in HPV(−) cells stably expressing control or multiple shRNAs to USP7 (**B**) or HPV(+) cells expressing control vector or USP7 (**C**). **D** and **E,** Cyclohexamide (CHX) chase in HN5 (**D**) and HN30 (**E**) HPV(−) cells expressing control or shRNA for USP7 (shUSP7). **F,** MG132 rescue in several HPV(−)/p16(−) cell types (HN5, HN30, and HN31) expressing control or shUSP7. Data are densitometry from immunoblots in Supplementary Fig. S2C and are presented as mean ± SEM. Comparisons performed using ANOVA with *post hoc* analysis adjusted for multiple comparisons. *, $P < 0.05$ versus control; +, $P < 0.05$ versus shUSP7. **G,** IP for TRIP12 and immunoblot for HA or TRIP12 in HN5 cells expressing Ub-tagged HA and either control vector, p16 alone or USP7 and p16.

combination led to an approximate 50% reduction in cell viability (**Fig. 3K**). Although doses of GNE-6640 alone had no effect on clonogenic survival, the combination of GNE-6640 and olaparib decreased colony formation over olaparib alone by over 50% (**Fig. 3L**).

To further examine both the relationship between USP7 and p16 and its functional consequences, we force expressed p16 in HN5 cells and found downregulation of USP7, TRIP12, and BRCA1 (**Fig. 3M**) and significantly increased radiosensitization (**Fig. 3N**). However, these effects were partially reversed by combined forced expression of both p16 and USP7 (**Fig. 3M** and **N**).

We next examined the ability of p16 to similarly modulate HR and sensitivity to PARP inhibition. Specifically, we found repression of HR following forced expression of p16 in HPV(−) cells (**Fig. 3O**) and enhanced sensitivity to olaparib on MTT (**Fig. 3P**) and clonogenic assay (**Fig. 3Q**). Conversely, knock-out of p16 in HPV(+) cells led to significantly more HR (**Fig. 3R**) and reduced sensitivity to olaparib (**Fig. 3S** and **T**).

P16 represses USP7 via transcriptional activation of HUWE1

To better understand how p16 might modulate USP7 ubiquitination, we identified binding partners of USP7 via immunoprecipitation mass spectrometry (IP/MS; schema in Supplementary Fig. S5A) with an IP for USP7 followed by identification of proteins bound to USP7 in 3 HPV(−)/p16 (−) cell lines (HN5, HN30 and HN31) and 3 HPV(+)/p16 (+) cell lines (UPCI:SCC-152, UPCI:SCC-154 and UM-SCC-47). We identified three E3 ubiquitin ligases (HUWE1, TRIM21, and RNF168) binding USP7 in all HPV(−) cell lines tested (Supplementary Fig. S5B, left column). For two of the HPV(+) cell lines (UPCI:SCC-152 and UPCI:SCC-154), USP7 had to be overexpressed before IP/MS due to insufficient levels of endogenous USP7. The HPV(+) cell lines had a similar set of binding partners with HUWE1 and TRIM21 binding USP7 in all 3 cell lines (Supplementary Fig. S5B). A reverse IP/MS, with an IP for HUWE1 confirmed its binding with USP7 in all cell types examined (Supplementary Fig. S5C).

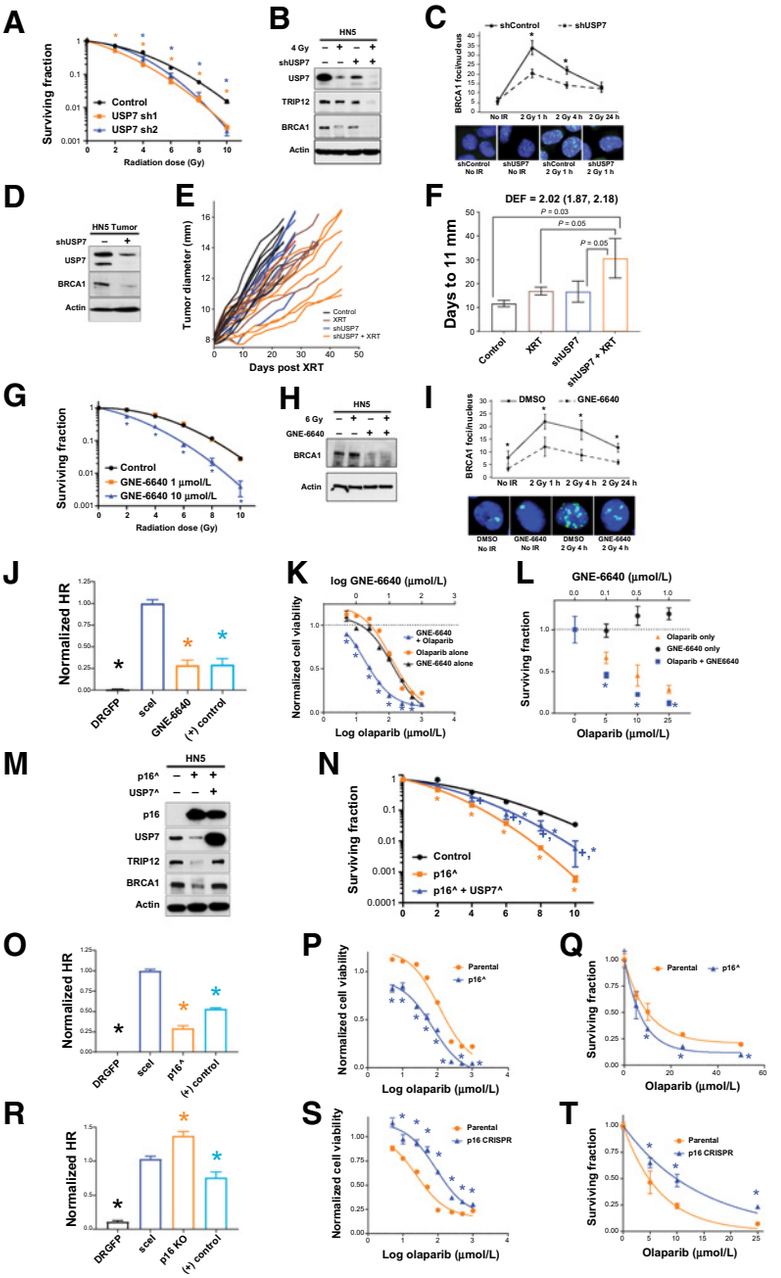

Figure 3.

p16 inhibits USP7, leading to increased sensitivity to radiotherapy and PARP inhibitor. **A–C,** Clonogenic survival assay (**A**), immunoblot (**B**), and BRCA1 foci (representative images shown; **C**) in HN5 HPV(−) cells stably expressing control or shUSP7 constructs. **D–F,** Following intramuscular injection of HN5 cells expressing control or shUSP7 and treatment with 4 Gy x 5 days, tumors were collected and subjected to immunoblot (**D**). **E,** Growth curves for each individual tumor are shown (n = 7/treatment group). **F,** Days for each tumor to reach 11 mm in diameter was calculated for each tumor based on the growth curve (**E**). **G–I,** Clonogenic survival assay (**G**), immunoblot (**H**), and BRCA1 foci formation (**I**) in HN5 cells treated with the USP7 inhibitor GNE-6640. **J,** HR assay in HN5 cells treated with GNE-6640. **K** and **L,** MTT (**K**) and clonogenic survival assay (**L**) in HN5 cells treated with GNE-6640 and/or olaparib. **M** and **N,** Immunoblot (**M**) and clonogenic survival assay (**N**) in HN5 cells stably expressing control vector, p16 or p16 and USP7. **O–Q,** HR Assay (**O**), MTT assay (**P**), and clonogenic assay (**Q**) in HN5 cells forced to express p16 and treated with olaparib. **R–T,** HR assay (**R**), MTT assay (**S**), and clonogenic assay (**T**) in UM-SCC-47 HPV(+) cells with p16 KO treated with olaparib at the indicated concentrations. DEF, dose enhancement factor of USP7 inhibition. Composite data are presented as mean ± SEM. Comparisons performed using ANOVA with *post hoc* analysis adjusted for multiple comparisons. *, $P < 0.05$ versus control.

To determine which of the identified E3 ubiquitin ligases may be regulating USP7, we initially performed immunoblots for HUWE1, TRIM21, USP7, TRIP12 and p16 (**Fig. 4A**). HUWE1 exhibited an inverse relationship to both USP7 and TRIP12 and correlated with p16/HPV positivity, suggesting that this E3 ubiquitin ligase could be limiting USP7 expression. Conversely, TRIM21 was less associated with USP7, TRIP12 or p16 expression.

We next examined mRNA expression of HUWE1 and TRIM21 and found that HUWE1 correlated with p16/HPV positivity, indicating that HUWE1 is likely transcriptionally regulated by p16 (**Fig. 4B**). However, TRIM21 did not exhibit the inverse correlation expected (**Fig. 4C**). In addition, we expressed p16 in HN5 cells, which led to an increase in both HUWE1 protein and mRNA levels (**Fig. 4D** and **E**). This finding confirms that p16 regulates HUWE1 at the transcriptional level. Conversely, inhibition of p16 in HPV(+) cells led to a decrease in HUWE1 gene expression (**Fig. 4F**).

To confirm the link between p16, HUWE1 and USP7, HN5 cells with forced expression of p16 were cotransfected with HUWE1, TRIM21, TRIP12 or USP7 siRNA. Immunoblotting showed that HUWE1 expression increased with forced p16 expression (**Fig. 4G**), whereas TRIM21 did not appear to be affected by p16 expression, again confirming that p16 regulates HUWE1 and not TRIM21. Most importantly, p16-induced downregulation of USP7 and TRIP12 was partially rescued by cotransfection of HUWE1 siRNA (**Fig. 4G**) or stable expression of HUWE1 shRNA (**Fig. 4H**),

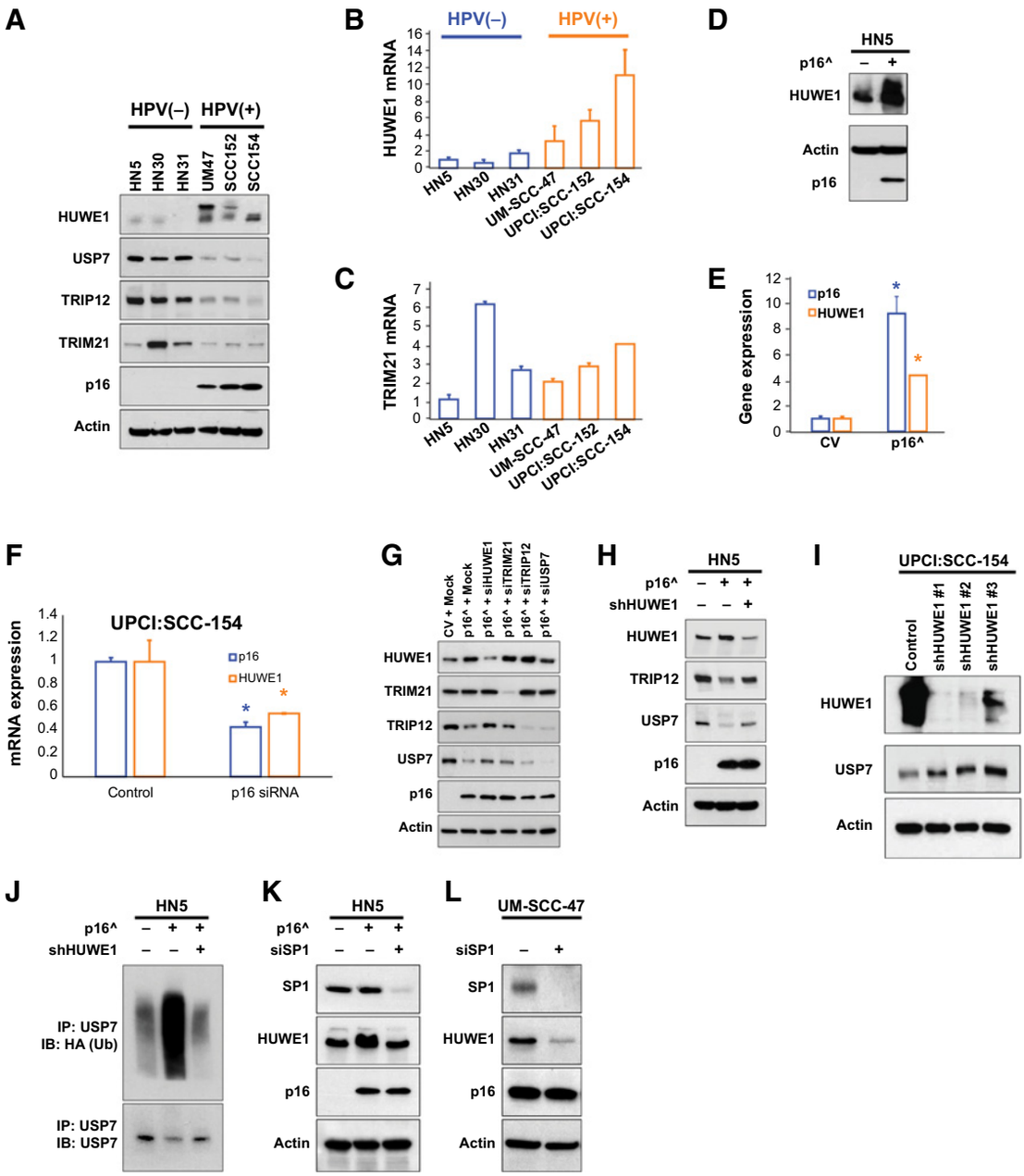

Figure 4.

p16 represses USP7 via transcriptional activation of HUWE1. **A–C,** Immunoblot (**A**) and RT-PCR for HUWE1 (**B**) and TRIM21 (**C**) in HNSCC cells. **D** and **E,** Immunoblot (**D**) and RT-PCR (**E**) in HN5 HPV(−) cells expressing control vector or p16. **F,** RT-PCR in UPCI:SCC-154 HPV(+) cells transfected with siRNA targeting p16. **G** and **H,** Immunoblot in HN5 cells expressing control vector or p16 and siRNA (**G**) or stably expressing control or HUWE1 shRNA (shHUWE1; **H**). **I,** Immunoblot in UPCI:SCC-154 HPV(+) cells stably expressing control or shRNA to HUWE1. **J,** IP for USP7 and immunoblot for HA in HN5 cells expressing HA-tagged Ub and control vector, p16 or p16 and shHUWE1. **K,** Immunoblot in HN5 cells expressing control vector, p16 or p16 and siRNA to SP1 (siSP1). **L,** Immunoblot in UM-SCC-47 cells expressing control or siSP1. Composite data are presented as mean ± SEM. The Student *t* test was used to compare control versus p16-modulated groups. *, $P < 0.05$ versus control for indicated gene.

confirming HUWE1 as an E3 ligase for USP7 downstream of p16. Moreover, in HPV(+) cells, inhibition of HUWE1 via siRNA led to an increase in USP7 (**Fig. 4I**), demonstrating the importance of HUWE1 in the repression of USP7 expression by p16 in HPV(+) HNSCC. In addition, forced expression of p16 in HN5 cells led to ubiquitination of USP7, which was rescued by cotransfection with HUWE1 shRNA, thus confirming that p16 regulates USP7 through its ubiquitination by HUWE1 (**Fig. 4J**).

To understand how p16 controls HUWE1 transcription, we examined the HUWE1 promoter region, which contains binding sites for

multiple enhancers and promoters, including specificity protein 1 (SP1). SP1 is a transcription factor and has been found to bind to p16, leading to increased transcriptional activity of the target gene but not total expression level (29). To determine whether SP1 is a mediator of p16-driven upregulation of HUWE1, we inhibited SP1 expression in either HPV(−) cells forced to express p16 (**Fig. 4K**) or HPV(+) cells (**Fig. 4L**). In the HPV(−) cells, HUWE1 levels increased as expected upon p16 expression, but this increase was reversed by SP1 inhibition (**Fig. 4K**). Similarly, inhibition of SP1 in HPV(+) cells led to a decrease in HUWE1 expression (**Fig. 4L**). Thus, our results suggest that SP1 transcriptional activity is potentially responsible for the p16-driven HUWE1 upregulation.

Decreased HUWE1 expression is associated with worse DFS in HPV(−) HNSCC

To determine whether HUWE1 is associated with outcomes in HNSCC, we examined both HUWE1 mutation and expression levels in TCGA HNSCC patient cohort and evaluated their DFS. We found that HUWE1 expression was elevated in HPV(+) tumors and reduced in the small number of tumors with truncating HUWE1 mutations (Supplementary Fig. S6). In patients with HPV(−), low HUWE1 expression as a continuous variable was associated with worse DFS in univariate analysis ($P = 0.018$) and remained significant in multivariate analysis, including tumor site and clinical stage ($P = 0.016$). When divided into groups by HUWE1 expression [top tertile (hi, blue line) vs. others (lo, orange line)], lower HUWE1 expression was associated with worse DFS ($P = 0.048$; **Fig. 5A**). This phenomenon was not observed in patients with HPV(+; **Fig. 5B**). Moreover, in patients with HPV(−), truncating mutations in HUWE1 were associated with a median DFS of 9.4 months compared with 67.7 months in the remaining patients ($P = 0.008$; **Fig. 5C**), whereas no effect was observed in patients with HPV(+; **Fig. 5D**). These data suggest that HUWE1 is present at high levels in clinical HPV(+) tumors, whereas its expression in HPV(−) HNSCC is repressed and associated with outcome and response to therapy.

Discussion

Here, we present evidence that HPV-driven p16 expression represses TRIP12 and HR via increased transcription of HUWE1, leading to ubiquitination and degradation of USP7 (Supplementary Fig. S7). This is the first report of a direct signaling relationship between p16, HUWE1, and USP7, elucidating the mechanism by which p16 inhibits DNA repair and the tumor cell response to DNA damage. In addition, activity of this p16-driven signaling cascade modulates sensitivity to PARP inhibition, whereas its repression—and subsequent activation of USP7—is druggable via USP7 inhibitors to promote radiosensitization.

Despite being a clinical surrogate for HPV positivity (15), the function of p16 in HPV(+) disease is unclear. p16 inhibits cell-cycle progression via suppression of CDK4/6-mediated phosphorylation of Rb. In most contexts, hypophosphorylated Rb binds to E2F

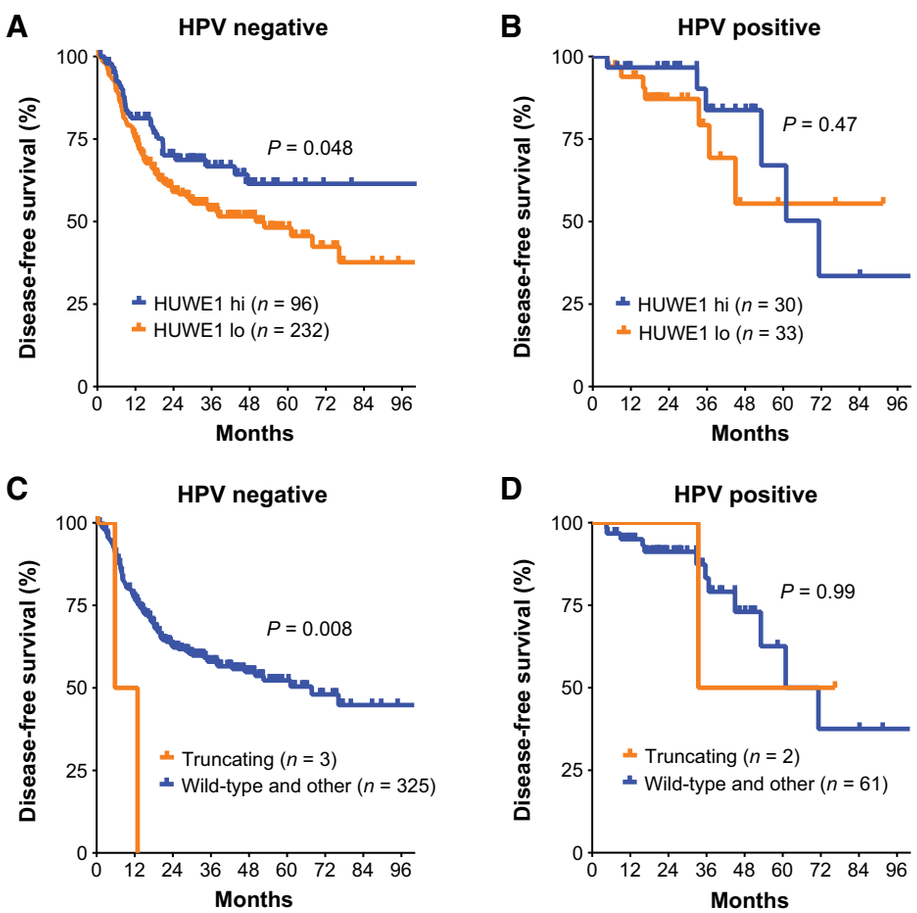

Figure 5.
Decreased HUWE1 expression is associated with worse DFS in HPV(−) HNSCC. Patients from the head and neck TCGA cohort were divided based upon HPV status, HUWE1 mRNA expression [topmost tertile (hi, blue line) vs. bottom two tertiles (lo, orange line)] and mutation [truncating (orange line) vs. other/wild type (blue line)], with number in each group indicated. DFS analyzed using log rank statistics, with *P* values shown.

family members, leading to their sequestration. This prevents expression of genes needed to enter S-phase, leading to cell-cycle arrest and potentially senescence (30). Indeed, repression of p16 expression can be a key aspect of tumorigenesis, contributing to uncontrolled proliferation (31, 32). Conversely, in HPV(+) tumors, Rb is inactivated by E7, resulting in a release of negative feedback control on p16 expression (33). Because of the inactivation of Rb in HPV(+) cells, p16 does not trigger cell-cycle arrest. Because of loss of canonical p16 function, high levels of p16 in HPV(+) disease are thought to be of minimal biologic consequence (33).

This understanding belies the fact that p16 can have functions beyond its effects on Rb, CDK4/6 and cell-cycle progression. For example, p16 binds to and attenuates HIF1α activity, leading to decreased VEGF and tumor angiogenesis (34, 35), and loss of p16 is tumorigenic in the absence of Rb possibly via increased genomic instability (36). In addition, both our group and others have shown that p16 inhibition potentiates DNA-damage in a CDK4/6 independent fashion (12, 37), partially explaining the relative radiosensitivity of HPV(+) tumors. Our work examining this phenomenon identified TRIP12 repression by p16 leading to increased radiosensitivity in HPV(+) tumors and high levels of TRIP12 expression in HPV(−) disease associated with radioresistance.

Unfortunately, although TRIP12 can drive radioresistance, it is not targetable. This deficit combined with the lack of biologically driven radiosensitizers available, drove us to identify additional upstream targets stabilizing TRIP12, with a goal of finding druggable drivers of radioresistance. By identifying p16-mediated repression of USP7 in HPV(+) cancer—leading to TRIP12 repression and sensitivity to radiotherapy—we were able to use pharmacological inhibitors of USP7 to recapitulate the radiosensitivity of HPV(+) cells in HPV(−) models. Our initial USP7 inhibitor, P5091, is not specific to USP7 but additionally inhibits USP47 (ubiquitin-specific peptidase 47), which, among several functions, controls tumor cell proliferation (38, 39). Although P5091 is under clinical evaluation for multiple myeloma, it is unclear whether a USP7 or USP47-based mechanism is responsible for its antineoplastic activity. Thus, for clinical translation of our findings, it will be necessary to develop more specific inhibitors of USP7. To this end, we evaluated GNE-6640, a more specific inhibitor of USP7 deubiquitinase activity (26). Although not yet in clinical trials, our data, as well as recent data linking USP7 inhibition to increased DNA damage (40), support further exploration of GNE-6640 as a means of targeting USP7 to radiosensitize HNSCC.

This radiosensitization appears to be due to a repression of BRCA1 and HR in the context of inhibition of USP7 (in the case of chemical or shRNA mediated inhibition) or basal repression of USP7 (in the presence of p16). This repression presents an additional avenue for targeted therapy in HNSCC. Specifically, the combination of USP7 and PARP inhibition led to potentiation of cytotoxicity at doses that had negligible effects on their own. Moreover, when p16 was modulated directly, its forced expression in HPV(−) cells inhibited HR and potentiated the cytotoxicity of PARP inhibition, whereas its inhibition in HPV(+) cells led to increased HR and resistance to PARP inhibition. This has significant implications for PARP inhibition in HNSCC, which has underperformed to some degree in clinical trials (41, 42).

It is known that in the context of BRCA1/2 mutation, HR is defective and DSBs are repaired via non-HR (NHEJ), which in turn confers sensitivity to therapies that lead to collapse of DNA replication forks (43). The most studied of these in the BRCA-mutated setting are the PARP inhibitors, which are FDA-approved for use in BRCA-mutated tumors (44, 45). However, the phenotype of the BRCA-mutated state has been expanded into the concept of "BRCAness," which can be attained by a variety of genetic alterations leading to repression of HR, such as a deficiency in ATR, ATM, and CHK1/2 (46). It is known that HPV(+) tumors exhibit a repression in HR, thought to be due to the relationship between the viral proteins E6 and E7 with HR-related proteins (47–49). However, E7 has been associated with the activation of multiple DDR-associated genes, such as ATM and ATR (50–54). Moreover, our work and that of others provide a direct link between p16 function and repression of HR (12, 55). This repression, coupled with our observation that the presence of p16 regulated sensitivity to PARP inhibition, provides an avenue for improving patient selection for PARP inhibitor application in HNSCC. In addition, although our own data and that of others do not suggest dramatic benefits of the combination of PARP inhibition and radiotherapy in unselected HPV(+) disease (11, 37), it does provide another link in explaining the heightened sensitivity of HPV(+) tumors to cisplatin and radiotherapy.

The connection between p16 and USP7 has not previously been established, and our results identified significant functional consequences of p16-USP7 signaling in the setting of therapeutic response. Therefore, we explored this connection and identified HUWE1 as a direct link between p16 and USP7. HUWE1 is a HECT, UBA and WWE domain containing E3 ubiquitin protein ligase 1 that is involved in the stress response, proliferation, differentiation, apoptosis, and DNA repair (56). As an E3 ligase, HUWE1 marks proteins, including the DNA repair proteins BRCA1 and H2AX, with ubiquitin for degradation through the proteasome, thus decreasing the DNA repair capacity of both HR and NHEJ. Because HUWE1 and USP7 were also discovered to bind in our cell lines via IP/MS analysis, the E3 ubiquitin ligase HUWE1 may be antagonistic to USP7 and play an intermediary role in the p16/TRIP12 pathway and the inhibition of BRCA1 function. As we demonstrated in this report, knockdown of HUWE1 rescued p16-dependent downregulation of USP7 at the protein and gene levels, validating this prediction.

Finally, the E3 ligase HUWE1 was found to be transcriptionally controlled partially via SP1 downstream of p16, connecting p16 to USP7 protein. Previously, it has been shown that p16 can form a complex with SP1, facilitating the transcriptional activity of the latter (29, 57). SP1 is one of several predicted transcription factors for HUWE1; however, our data are the first to our knowledge to show this regulation in any context, particularly in a p16-driven fashion.

Although our data do not rule out regulation of HUWE1 by p16 via other means, they do provide a direct link between p16 and HUWE1, rounding out a potentially complete pathway. In addition, although we uncovered the roles of USP7 and HUWE1 in the p16-driven pathway responsible for regulating DNA damage partially via TRIP12, it is also possible that additional deubiquitinases control TRIP12 cellular levels and could act as intermediaries between p16 and TRIP12, leaving open possibilities for inherent or acquired therapeutic resistance. Finally, HPV(+) and HPV(−) cells differ in both mutational spectra and epigenetic features, in addition to their differential p16 status, thus forced expression of p16 in the HPV(−) context likely does not fully recapitulate the HPV(+) cell. However, as HPV(−) cells are generally far more radioresistant than HPV(+) cells, identifying USP7 as a targetable mediator of radioresistance via this pathway could be highly significant. Moreover, inhibition of p16 in HPV-positive cells does both modulate HUWE1-USP7 signaling as well as render HPV(+) cells more resistant to radiotherapy and olaparib, arguing for the applicability of this pathway in the HPV(+) context.

In conclusion, we identified a signaling pathway connecting p16 expression in HPV(+) cells to repression of HR via transcriptional upregulation of HUWE1 followed by ubiquitin-dependent signaling to

USP7, which further downregulates TRIP12 and BRCA1. This pathway is clinically important—as evidenced by the relationship between HUWE1 and clinical outcome—and targetable. In HPV(+) tumors, the activity of this pathway may be related to a "BRCAness" and increased sensitivity to agents that target HR—such as PARP inhibition—thus providing a potential biomarker for their effectiveness. Conversely, the inhibitors of USP7 could be used to engender this "BRCAness" in HPV(−) tumors rendering them sensitive to radiotherapy as well as PARP inhibition. Thus, our findings have wide implications for most solid tumors and could lead to a rethinking of the role of p16 in therapeutic response.

Authors' Disclosures

C.R. Pickering reports grants from National Institutes of Health (NIH) during the conduct of the study and National Institutes of Health (NIH) outside the submitted work. H.D. Skinner reports grants from National Cancer Institute, Cancer Prevention Institute of Texas, and National Institute for Dental and Craniofacial Research during the conduct of the study. No disclosures were reported by the other authors.

Authors' Contributions

D.P. Molkentine: Conceptualization, investigation, methodology, writing–original draft, writing–review and editing. **J.M. Molkentine:** Conceptualization, investigation, visualization, methodology, writing–original draft, writing–review and editing. **K.A. Bridges:** Investigation, writing–review and editing. **D.R. Valdecanas:** Investigation, methodology, writing–review and editing. **A. Dhawan:** Investigation, writing–review and editing. **R. Bahri:** Investigation, writing–review and editing. **A.J. Hefner:** Investigation, writing–review and editing. **M. Kumar:** Investigation, writing–review and editing. **L. Yang:** Investigation, writing–review and editing. **M. Abdelhakiem:** Investigation, writing–review and editing. **P.M. Pifer:** Conceptualization, writing–review and editing. **V. Sandulache:** Methodology, writing–review and editing. **A. Sheth:** Investigation, writing–review and editing. **B.M. Beadle:** Methodology, writing–review and editing. **H.D. Thames:** Methodology, writing–review and editing. **K.A. Mason:** Supervision, methodology, project administration. **C.R. Pickering:** Conceptualization, funding acquisition, writing–review and editing. **R.E. Meyn:** Conceptualization, methodology, project administration. **H.D. Skinner:** Conceptualization, supervision, funding acquisition, investigation, visualization, methodology, writing–original draft, project administration, writing–review and editing.

Acknowledgments

IP/MS performed with help from Dr. D. Hawke funded in part by the NIH/NCI Cancer Center Support Grant (CCSG) #P30CA016672, the NIH High-End Instrumentation program grant #1S10OD012304–01, and CPRIT Core Facility Grant #RP130397. Supported by (i) the National Cancer Institute R01CA168485–08 and P50CA097190–15 (to H.D. Skinner), (ii) the National Institute for Dental and Craniofacial Research R01DE028105 (to H.D. Skinner) and R01DE028061 (to H.D. Skinner and C.R. Pickering), (iii) The Cancer Prevention Institute of Texas RP150293 (to H.D. Skinner and C.R. Pickering), and (iv) Veterans Administration Clinical Science Research and Development Division Career Development Award 1IK2CX001953 (to V. Sandulache). The authors thank Drs. A. Faust and A. Clemens for editorial assistance. Pathway and IP/MS figures generated using Biorender (https://app.biorender.com/).

The costs of publication of this article were defrayed in part by the payment of page charges. This article must therefore be hereby marked *advertisement* in accordance with 18 U.S.C. Section 1734 solely to indicate this fact.

Received July 2, 2021; revised October 7, 2021; accepted December 27, 2021; published first December 29, 2021.

References

1. Viens LJ. Human papillomavirus–associated cancers—United States, 2008–2012. MMWR Morb Mortal Wkly Rep [Internet]. 2016 [cited 2020 May 6];65. Available from: https://www.cdc.gov/mmwr/volumes/65/wr/mm6526a1.htm.
2. Zandberg DP, Bhargava R, Badin S, Cullen KJ. The role of human papillomavirus in nongenital cancers. CA Cancer J Clin 2013;63:57–81.
3. Arbyn M, de Sanjosé S, Saraiya M, Sideri M, Palefsky J, Lacey C, et al. EUROGIN 2011 roadmap on prevention and treatment of HPV-related disease. Int J Cancer 2012;131:1969–82.
4. de Martel C, Plummer M, Vignat J, Franceschi S. Worldwide burden of cancer attributable to HPV by site, country and HPV type: worldwide burden of cancer attributable to HPV. Int J Cancer 2017;141:664–70.
5. Stein AP, Saha S, Kraninger JL, Swick AD, Yu M, Lambertg PF, et al. Prevalence of human papillomavirus in oropharyngeal cancer: a systematic review. Cancer J 2015;21:138–46.
6. Senkomago V, Henley SJ, Thomas CC, Mix JM, Markowitz LE, Saraiya M. Human papillomavirus-attributable cancers—United States, 2012–2016. MMWR Morb Mortal Wkly Rep 2019;68:724–8.
7. Ang KK, Harris J, Wheeler R, Weber R, Rosenthal DI, Nguyen-Tân PF, et al. Human papillomavirus and survival of patients with oropharyngeal cancer. N Engl J Med 2010;363:24–35.
8. Gillison ML, D'Souza G, Westra W, Sugar E, Xiao W, Begum S, et al. Distinct risk factor profiles for human papillomavirus type 16–positive and human papillomavirus type 16–negative head and neck cancers. J Natl Cancer Inst 2008;100:407–20.
9. Busch CJ, Kriegs M, Laban S, Tribius S, Knecht R, Petersen C, et al. HPV-positive HNSCC cell lines but not primary human fibroblasts are radiosensitized by the inhibition of Chk1. Radiother Oncol 2013;108:495–9.
10. Rieckmann T, Tribius S, Grob TJ, Meyer F, Busch CJ, Petersen C, et al. HNSCC cell lines positive for HPV and p16 possess higher cellular radiosensitivity due to an impaired DSB repair capacity. Radiother Oncol 2013;107:242–6.
11. Molkentine JM, Molkentine DP, Bridges KA, Xie T, Yang L, Sheth A, et al. Targeting DNA damage response in head and neck cancers through abrogation of cell-cycle checkpoints. Int J Radiat Biol 2020;1–8.
12. Wang L, Zhang P, Molkentine DP, Chen C, Molkentine JM, Piao H, et al. TRIP12 as a mediator of human papillomavirus/p16-related radiation enhancement effects. Oncogene 2017;36:820–8.
13. Kimple RJ, Smith MA, Blitzer GC, Torres AD, Martin JA, Yang RZ, et al. Enhanced radiation sensitivity in HPV-positive head and neck cancer. Cancer Res 2013;73:4791–800.
14. Mirghani H, Amen F, Tao Y, Deutsch E, Levy A. Increased radiosensitivity of HPV-positive head and neck cancers: molecular basis and therapeutic perspectives. Cancer Treat Rev 2015;41:844–52.
15. Lewis JS, Beadle B, Bishop JA, Chernock RD, Colasacco C, Lacchetti C, et al. Human papillomavirus testing in head and neck carcinomas: guideline from the college of American pathologists. Arch Pathol Lab Med 2018;142:559–97.
16. Klussmann JP, Gultekin E, Weissenborn SJ, Wieland U, Dries V, Dienes HP, et al. Expression of p16 protein identifies a distinct entity of tonsillar carcinomas associated with human papillomavirus. Am J Pathol 2003;162:747–53.
17. El-Naggar AK, Westra WH. p16 expression as a surrogate marker for HPV-related oropharyngeal carcinoma: a guide for interpretative relevance and consistency. Head Neck 2012;34:459–61.
18. Hall M, Bates S, Peters G. Evidence for different modes of action of cyclin-dependent kinase inhibitors: p15 and p16 bind to kinases, p21 and p27 bind to cyclins. Oncogene 1995;11:1581–8.
19. Matsumura Y, Yamagishi N, Miyakoshi J, Imamura S, Takebe H. Increase in radiation sensitivity of human malignant melanoma cells by expression of wild-type p16 gene. Cancer Lett 1997;115:91–6.
20. Lee AW, Li JH, Shi W, Li A, Ng E, Liu TJ, et al. p16 gene therapy: a potentially efficacious modality for nasopharyngeal carcinoma. Mol Cancer Ther 2003;2:961–9.
21. Kawabe S, Roth JA, Wilson DR, Meyn RE. Adenovirus-mediated p16INK4a gene expression radiosensitizes non–small cell lung cancer cells in a p53-dependent manner. Oncogene 2000;19:5359–66.
22. Mirzayans R, Andrais B, Hansen G, Murray D. Role of p16(INK4A) in replicative senescence and DNA damage-induced premature senescence in p53-deficient human cells. Biochem Res Inter 2012;2012:951574.

23. Gudjonsson T, Altmeyer M, Savic V, Toledo L, Dinant C, Grofte M, et al. TRIP12 and UBR5 suppress spreading of chromatin ubiquitylation at damaged chromosomes. Cell 2012;150:697–709.
24. Liu X, Yang X, Li Y, Zhao S, Li C, Ma P, et al. Trip12 is an E3 ubiquitin ligase for USP7/HAUSP involved in the DNA damage response. FEBS Lett 2016;590: 4213–22.
25. Ramadan K, Meerang M. Degradation-linked ubiquitin signal and proteasome are integral components of DNA double-strand break repair: new perspectives for anti-cancer therapy. FEBS Lett 2011;585:2868–75.
26. Kategaya L, Di Lello P, Rougé L, Pastor R, Clark KR, Drummond J, et al. USP7 small-molecule inhibitors interfere with ubiquitin binding. Nature 2017;550: 534–8.
27. Altun M, Kramer HB, Willems LI, McDermott JL, Leach CA, Goldenberg SJ, et al. Activity-based chemical proteomics accelerates inhibitor development for deubiquitylating enzymes. Chem Biol 2011;18:1401–12.
28. Ritorto MS, Ewan R, Perez-Oliva AB, Knebel A, Buhrlage SJ, Wightman M, et al. Screening of DUB activity and specificity by MALDI-TOF mass spectrometry. Nat Commun 2014;5:4763.
29. Al-Khalaf HH, Mohideen P, Nallar SC, Kalvakolanu DV, Aboussekhra A. The cyclin-dependent kinase inhibitor p16INK4a physically interacts with transcription factor Sp1 and cyclin-dependent kinase 4 to transactivate microRNA-141 and microRNA-146b-5p spontaneously and in response to ultraviolet light-induced DNA damage. J Biol Chem 2013; 288:35511–25.
30. Romagosa C, Simonetti S, López-Vicente L, Mazo A, Lleonart ME, Castellvi J, et al. p16 Ink4a overexpression in cancer: a tumor-suppressor gene associated with senescence and high-grade tumors. Oncogene 2011;30:2087–97.
31. Ciriello G, Miller ML, Aksoy BA, Senbabaoglu Y, Schultz N, Sander C. Emerging landscape of oncogenic signatures across human cancers. Nature Genetics 2013; 45:1127–33.
32. Ko A, Han SY., Song J. Regulatory network of ARF in cancer development. Mol Cells 2018;41:381–9.
33. Chung CH, Gillison ML. Human papillomavirus in head and neck cancer: its role in pathogenesis and clinical implications. Clin Cancer Res 2009;15:6758–62.
34. Zhang J, Lu A, Li L, Yue J, Lu Y. p16 Modulates VEGF expression via its interaction with HIF-1α in breast cancer cells. Cancer investigation. NIH Public Access; 2010;28:588.
35. Baruah P, Lee M, Wilson POG, Odutoye T, Williamson P, Hyde N, et al. Impact of p16 status on pro- and anti-angiogenesis factors in head and neck cancers. Br J Cancer 2015;113:653.
36. Sen M, Akeno N, Reece A, Miller AL, Simpson DS, Wikenheiser-Brokamp KA. p16 controls epithelial cell growth and suppresses carcinogenesis through mechanisms that do not require RB1 function. Oncogenesis. Nature Publishing Group; 2017;6:e320–.
37. Dok R, Bamps M, Glorieux M, Zhao P, Sablina A, Nuyts S. Radiosensitization approaches for HPV-positive and HPV-negative head and neck squamous carcinomas. Int J Cancer 2020;146:1075–85.
38. Yan S, Yue Y, Wang J, Li W, Sun M, Gu C, et al. LINC00668 promotes tumorigenesis and progression through sponging miR-188–5p and regulating USP47 in colorectal cancer. Eur J Pharmacol 2019;858:172464.
39. Yu L, Dong L, Wang Y, Liu L, Long H, Li H, et al. Reversible regulation of SATB1 ubiquitination by USP47 and SMURF2 mediates colon cancer cell proliferation and tumor progression. Cancer Lett 2019;448:40–51.
40. Galarreta A, Valledor P, Ubieto-Capella P, Lafarga V, Zarzuela E, Muñoz J, et al. USP7 limits CDK1 activity throughout the cell cycle. EMBO J John Wiley & Sons, Ltd.; 2021;n/a:e99692.
41. Karam SD, Reddy K, Blatchford PJ, Waxweiler T, DeLouize AM, Oweida A, et al. Final report of a phase i trial of olaparib with cetuximab and radiation for heavy smoker patients with locally advanced head and neck cancer. Clin Cancer Res 2018;24:4949–59.
42. Psyrri A, Economopoulou P, Kotsantis I, Koutsodontis G, Cheila M, Papaxoinis G, et al. A phase II window of opportunity study of preoperative olaparib (O) with cisplatin (C) or durvalumab (D) or olaparib alone in in patients with operable squamous cell head and neck carcinoma (HNSCC; OPHELIA). Ann Oncol 2018;29:viii372.
43. Prakash R, Zhang Y, Feng W, Jasin M. Homologous recombination and human health: the roles of BRCA1, BRCA2, and associated proteins. Cold Spring Harb Perspect Biol 2015;7:a016600.
44. Bryant HE, Schultz N, Thomas HD, Parker KM, Flower D, Lopez E, et al. Specific killing of BRCA2-deficient tumours with inhibitors of poly(ADP-ribose) polymerase. Nature 2005;434:913–7.
45. Farmer H, McCabe N, Lord CJ, Tutt ANJ, Johnson DA, Richardson TB, et al. Targeting the DNA repair defect in BRCA mutant cells as a therapeutic strategy. Nature 2005;434:917–21.
46. McCabe N, Turner NC, Lord CJ, Kluzek K, Bialkowska A, Swift S, et al. Deficiency in the repair of DNA damage by homologous recombination and sensitivity to poly(ADP-ribose) polymerase inhibition. Cancer Res 2006;66: 8109–15.
47. Wallace NA, Khanal S, Robinson KL, Wendel SO, Messer JJ, Galloway DA. High-risk alphapapillomavirus oncogenes impair the homologous recombination pathway. J Virol 91:e01084–17.
48. Khanal S, Galloway DA. High-risk human papillomavirus oncogenes disrupt the Fanconi anemia DNA repair pathway by impairing localization and deubiquitination of FancD2. PLoS Pathog 2019;15:e1007442.
49. Wallace NA. Catching HPV in the homologous recombination cookie jar. Trends Microbiol 2020;28:191–201.
50. Moody CA, Laimins LA. Human papillomaviruses activate the ATM DNA damage pathway for viral genome amplification upon differentiation. PLoS Pathog 2009;5:e1000605.
51. Banerjee NS, Wang H-K, Broker TR, Chow LT. Human papillomavirus (HPV) E7 induces prolonged G_2 following S phase reentry in differentiated human keratinocytes. J Biol Chem 2011;286:15473–82.
52. Spardy N, Duensing A, Charles D, Haines N, Nakahara T, Lambert PF, et al. The human papillomavirus type 16 E7 oncoprotein activates the fanconi anemia (FA) pathway and causes accelerated chromosomal instability in FA cells. J Virol 2007; 81:13265–70.
53. Spardy N, Duensing A, Hoskins EE, Wells SI, Duensing S. HPV-16 E7 reveals a link between DNA replication stress, fanconi anemia D2 protein, and alternative lengthening of telomere–associated promyelocytic leukemia bodies. Cancer Res 2008;68:9954–63.
54. Hong S, Cheng S, Iovane A, Laimins LA. STAT-5 Regulates transcription of the topoisomerase IIβ-binding protein 1 (TopBP1) gene to activate the ATR pathway and promote human papillomavirus replication. mBio 2015;6: e02006–02015.
55. Dok R, Kalev P, Limbergen EJV, Asbagh LA, Vázquez I, Hauben E, et al. p16INK4a impairs homologous recombination–mediated DNA repair in human papillomavirus–positive head and neck tumors. Cancer Res 2014;74:1739–51.
56. Kao S-H, Wu H-T, Wu K-J. Ubiquitination by HUWE1 in tumorigenesis and beyond. J Biomed Sci 2018;25:67.
57. Buj R, Aird KM. p16: cycling off the beaten path. Mol Cell Oncol [Internet]. 2019 [cited 2020 Dec 17];6. Available from: https://www.ncbi.nlm.nih.gov/pmc/articles/PMC6816386/.